# Synthesis and luminescence properties of electrodeposited ZnO films

C. V. Manzano, D. Alegre, O. Caballero-Calero, B. Alén, and M. S. Martín-González[a)]
*IMM-Instituto de Microelectrónica de Madrid (CNM-CSIC), Isaac Newton 8, PTM, E-28760 Tres Cantos, Madrid, Spain*

(Received 22 March 2011; accepted 6 July 2011; published online 31 August 2011)

Zinc oxide (ZnO) films have been grown on gold (111) by electrodeposition using two different $OH^-$ sources, nitrate and peroxide, in order to obtain a comparative study between them. The morphology, structural and optical characterization of the films were investigated depending on the solution used (nitrate and peroxide) and the applied potential. Scanning electron microscopy pictures show different morphologies in each case. X-ray diffraction confirms that the films are pure ZnO oriented along the (0002) direction. ZnO films have been studied by photoluminescence to identify the emission of defects in the visible range. A consistent model that explains the emissions for the different electrodeposited ZnO films is proposed. We have associated the *green and yellow emissions* to a transition from the donor $OH^-$ to the acceptor zinc vacancies ($V_{Zn}^-$) and to interstitial oxygen ($O_i^0$), respectively. The *orange-red emission* is probably due to transitions from the conducting band to $O_i^-$ and $O_{Zn}^0$ defects and the *infrared emission* to transition from these $O_i^{-/2-}$ and $O_{Zn}^{0/-}$ defects to the valence band. © *2011 American Institute of Physics*. [doi:10.1063/1.3622627]

## I. INTRODUCTION

There has been a great interest in zinc oxide (ZnO) in recent years because it is a material with remarkable and varied properties. Due to its wide bandgap (3.36 eV), it is transparent in the visible range. It has a large exciton energy (60 meV) which implies that excitonic laser action of ZnO can be observed above room temperature. In addition, it has a multicolored visible emission depending on the growth conditions.[1] These characteristics provide an efficient emission in the ultraviolet and visible ranges, even at room temperature. Among other interesting properties, ZnO is a piezoelectric material, has a great magneto-optical effect, behaves as a good chemical sensor,[2,3] and is biocompatible and biosafe.[4,5] Moreover, when doped with Al, it presents a large power factor (high figure of merit ZT) at high temperatures when compared to other metal oxides.[6] More recently, this semiconductor has been the subject of intense research due to the appearance of ferromagnetism when it is "doped" with transition metals. These metals have been deemed room temperature diluted magnetic semiconductors, although it has been demonstrated that this effect could also be due to interfacial electrochemical reactions and interfaces effects.[7–12] As a consequence of those varied properties, ZnO can be used in cantilevers for atomic force microscopes,[13] dye sensitized solar cells,[14,15] sun creams, and as a white light emitting diodes (LEDs).[16,17] Finally, several groups have fabricated homojunctions with ZnO, obtaining emission of different colors such as blue-violet[18] and blue-yellow.[19] Also, UV photodiodes have been reported in the literature.[20] Other colors observed from heterojunctions with ZnO were UV,[21,22] violet-white,[23] blue-white, and white.[24]

As far as the growth method is concerned, there are multiple ways of obtaining ZnO films, such as chemical vapor deposition, metalorganic chemical vapor deposition, sputtering, molecular beam epitaxy, and pulsed laser deposition. The main drawback of the above-mentioned techniques is that they require ultrahigh vacuum and, in some cases, high temperatures. A way to avoid these constraints is to use other kinds of fabrication methods, such as chemical bath deposition or electrodeposition. In this sense, doped and undoped ZnO have been grown by electrodeposition in a successful and controlled way.[25] The electrodeposition is a large area approach, which provides, in principle, the same type of emitting ZnO nanorods as the aqueous chemical growth since it is also a low temperature process. However, it has the advantage of selective area growth by the prestructuring of the metallic substrate; therefore, it is of great interest for applications requiring the integration of LEDs in specific areas. This factor reduces one of the processing steps when making ZnO nanorod based devices.[12]

Electrodeposition of ZnO is usually performed using solutions with an acidic *p*H. The process implies the electrochemical formation of hydroxide ions at the surface of the working electrode. These ions react with the zinc ions present in the solution to form zinc oxide by means of the dehydration of zinc hydroxide at temperatures greater than 50 °C.[26] The general reaction is

$$Zn^{2+} + 2OH^- \leftrightarrow Zn(OH)_2 \leftrightarrow ZnO + H_2O. \quad (1)$$

The hydroxide ions ($OH^-$), which act as the precursors for the formation of zinc hydroxide, can be electrochemically obtained via three different ways:[26,27]

$$(1/2)O_2 + H_2O + 2e^- \leftrightarrow 2OH^-, \quad (2)$$

$$NO_3^- + H_2O + 2e^- \leftrightarrow NO_2^- + 2OH^-, \quad (3)$$

$$H_2O_2 + 2e^- \leftrightarrow 2OH^-. \quad (4)$$

[a)]Author to whom correspondence should be addressed. Electronic mail: marisol@imm.cnm.csic.es.

 

The first studies made about the electrochemical deposition of zinc oxide were published at the same time by two independent groups: Peulon and Lincot,[28] who used dissolved oxygen, and Izaki and Omi,[29] who used nitrate. Later on, Pauporté and Lincot developed and studied the mechanism of another different precursor: hydrogen peroxide.[27,30] This precursor presents two main advantages over the ones previously used: larger deposition velocity due to its great solubility in water (which was the main disadvantage when dissolved oxygen was used) and it does not generate any secondary reaction product (which was a problem when nitrate ions were present). Nevertheless, all these reactions are reversible, giving rise to quasiequilibrium conditions along the growth process. This explains the high crystalline quality achieved by electrodeposition of ZnO, quite similar to that obtained by means of other more expensive techniques, such as the ones previously mentioned. Also, it is interesting to note that the production of the oxide is direct without further thermal treatment as it is normal for most oxides.[31,32]

In this work, we present, to the best of our knowledge, the first comparative study of the quality of the films using different $OH^-$ sources. Both the morphology and the photoluminescence emission of electrodeposited ZnO films have been studied. Furthermore, a consistent model that explains the luminescence emissions of the defects present in electrodeposited ZnO films is also presented.

## II. EXPERIMENTAL

The electrochemical deposition has been performed with a standard electrochemical cell with a three electrode configuration: a platinum mesh as anode, a silver–silver chloride (Ag/AgCl 3M) electrode as reference electrode [$E_0 = +0.208$ V versus mormal hydrogen electrode (NHE)], and a thin film of 150 nm gold (111) electron beam evaporated on a silicon substrate (100) working electrode or cathode. The cell was controlled with a bi-potentiostat (Eco Chemie, Model AUT302.0) that was computer operated.

In order to perform the electrodeposition of the ZnO thin films, two different solutions of high purity (99.999%, Sigma-Aldrich Co.) zinc salts have been used. The other reactants are reagent grade potassium chloride from Panreac Química, S.A.U. and reagent grade stabilized 30% hydrogen peroxide from Panreac Química, S.A.U. The *nitrate solution contained* 0.1 M $Zn(NO_3)_2$ in de-ionized water (<14 mS) and the p*eroxide solution was prepared by* 5mM $ZnCl_2 + 0.04$ M $H_2O_2 + 0.1$ M KCl in de-ionized water (<14 mS).

The ZnO films were grown in a thermostatic bath at 80 °C with a thermal stability of ±1 °C. The electrodeposition was carried out in the following conditions:

(a) Nitrate solution—ZnO films were deposited potentiostatically at −1.0, −0.85, −0.7, and −0.6 V versus Ag/AgCl for 1 h.
(b) Peroxide solution—ZnO films were deposited potentiostatically for 1 h at different potentials. The chosen potentials were −0.9, −0.7, −0.5, and −0.3 V.

With regard to the characterization techniques used in this work, they can be divided into two groups. First, the morphology characterization of the films was performed using scanning electron microscopy (SEM) with a Hitachi S-800 and X-ray diffraction (XRD) spectroscopy with a Philips X-Pert Cuα X-ray transmitter four circle diffractometer. Second, the defect characterization was carried out via photoluminescence (PL) measurements. The samples were excited with a pulsed Nd:YAG tripled laser (355 nm wavelength, 15 ns pulse, 20 kHz repetition rate) modulated in intensity with an optical modulator (177 Hz). Then, the light emitted in the ultraviolet and/or visible range was filtered by suitable long pass filters and dispersed by a monochromator with 300 mm focal length (diffraction grating: 1200 lines/mm) and detected by means of a cooled photomultiplier, connected to a lock-in amplifier.

## III. RESULTS AND DISCUSSION

### A. ZnO deposition

As mentioned before, two different sources have been employed to obtain the hydroxide ions ($OH^-$) at the surface of the cathode: $NO_3^-$ and $H_2O_2$. Both cyclic voltammograms are shown in Fig. 1.

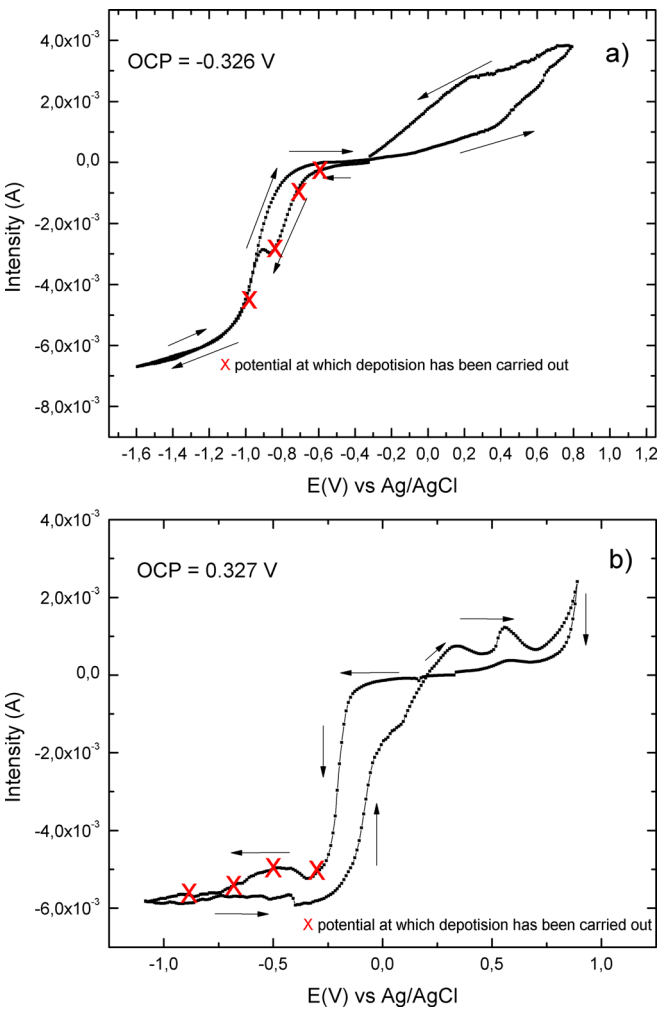


FIG. 1. (Color online) Linear voltammetric curves of (a) solution in 0.1 M $Zn(NO_3)_2$ and (b) in 5 mM $ZnCl_2 + 0.04$ M $H_2O_2 + 0.1$ M KCl. Scan rate = 0.01V $s^{-1}$, reference electrode Ag/AgCl.

In the case of the nitrate solution, Fig. 1(a), the deposition process of zinc hydroxide from a zinc nitrate solution is based on the reduction of the nitrate. A reduction peak at potentials around − 0.85 V versus Ag/AgCl is observed. This peak should be related to the reduction of $NO_3^-$.

The thermodynamically stable specie of this solution is ammonium ion ($NH_4^+$) (Ref. 33) at a *p*H of 4.5. However, the presence of $NO_2^-$ is the specie normally described in the literature,[34–39] according to the following reaction:

$$NO_3^- + H_2O + 2e^- \rightarrow NO_2^- + 2OH^-, \quad E^\circ = 0.835 - 0.0591\, pH \text{ vs NHE}. \tag{5a}$$

Although $NO_2^-$ is not thermodynamically stable under the present conditions, the kinetic of further reduction to ammonium ion is slow. However, reaction (5b) can occur with time producing more $OH^-$ according to the reaction:

$$NO_2^- + 6H_2O + 6e^- \rightarrow NH_4^+ + 8OH^-, \quad E^\circ = 0.897 - 0.0788\, pH \text{ vs NHE}. \tag{5b}$$

Thus, the mechanism for cathodic reduction of nitrate follows a consecutive reaction pathway $NO_3^- \rightarrow NO_2^- \rightarrow NH_4^+$. Therefore, reduction to ammonium ions should also be taken into account for long deposition times. In fact, Yu and Kupferle[40] studied the reduction of $NO_3^-$ ions at room temperature and concluded that nitrite ($NO_2^-$) accumulation was favored at less negative potentials and shorter deposition times, while ammonium formation was favored at more negative potentials and longer deposition times. The kinetics of disappearance of nitrite in our case should be faster than in that work since in our case the experiment is performed at 80 °C to obtain the ZnO directly.

After the reduction peak at − 0.85 V, the diminishing of the current in the voltammogram is attributed to the precipitation of ZnO observed experimentally on the electrode surface.

In this case, different films were deposited at − 1.0, − 0.85, − 0.7, and − 0.6 V versus Ag/AgCl at 80 °C and in all of them the presence of pure ZnO oriented along [0001] direction was detected by XRD (see Fig. 3 and the discussion in Sec. III B). No deposit was obtained at potentials less negative than − 0.5 V. Only the more representative results are presented in this study.

In the case of the peroxide solution, Fig. 1(b), the deposition process of zinc hydroxide is based on the reduction of the $H_2O_2$. This reduction takes place initially at *p*H = 5.8. A possible general reduction could be

$$H_2O_2 + H^+ + e^- \rightarrow OH_{(ad)} + H_2O, \tag{6a}$$

where (ad) stands for adsorbed. Equation (6a) is reported in the literature as a step process followed by a final desorption step[27]:

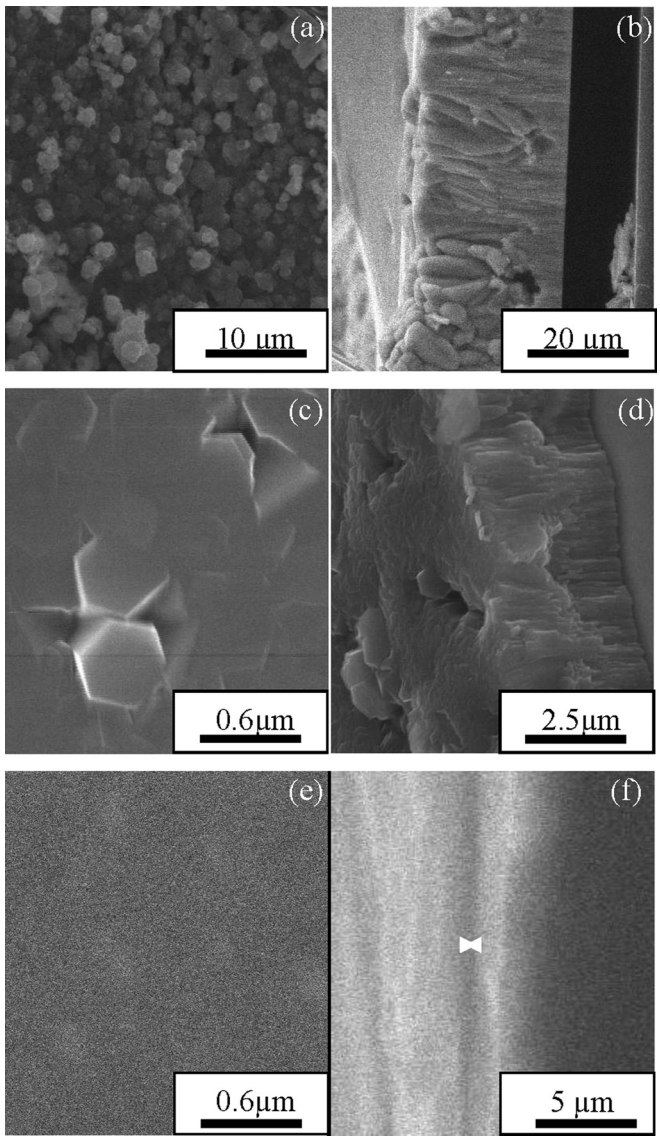


FIG. 2. SEM images of the films electrodeposited in the nitrate solution for 1 h; (a) − 1.0 V top view; (b) − 1.0 V 45° tilted view; (c) − 0.7 V top view; (d) − 0.7 V 45° tilted view; (e) − 0.6 V top view; (f) − 0.6 V cross section, the two arrows mark the film thickness.

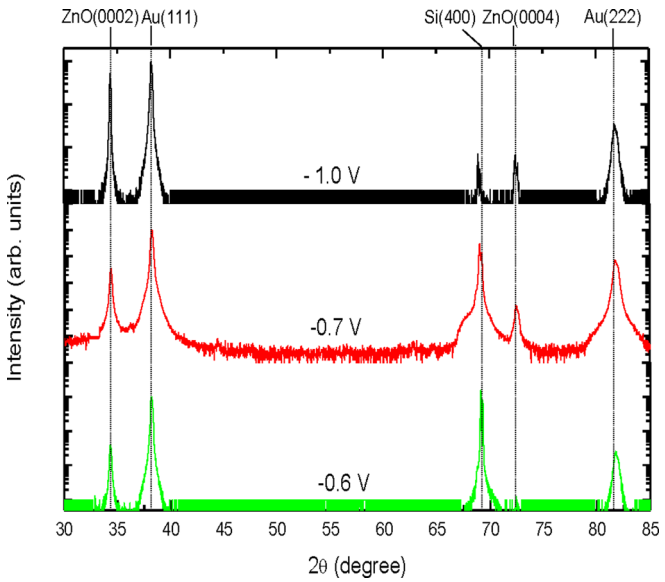


FIG. 3. (Color online) XRD patterns of the ZnO films grown in the nitrate solution at different voltages: − 1.0, − 0.7, and − 0.6 V vs Ag/AgCl.

$$H_2O_2 + H^+ + e^- \rightarrow OH_{(ad)} + H_2O, \quad (6b)$$

$$H_2O_2 + H^+ + OH_{(ad)} + e^- \rightarrow 2OH_{(ad)} + H_2O, \quad (6c)$$

$$OH_{(ad)} \rightarrow OH^-{}_{(dis)}, \quad (6d)$$

where (dis) stands for in solution.

In this case, different films were deposited at $-0.9$, $-0.7$, $-0.5$, and $-0.3$ V versus Ag/AgCl at 80 °C and in them the presence of pure ZnO was detected by XRD. No deposit was obtained at less negative potentials than $-0.2$ V. Only the more representative results are presented in this study.

## B. Quality and properties of ZnO films obtained

### 1. Nitrate solution

SEM micrographs of the films electrodeposited with the nitrate solution are shown in Fig. 2. As can be seen there, the morphology of the deposited film depends on the applied potential during deposition. For the most negative potentials [−1 V, Fig. 2(a)] rough films are obtained. That means that the growth was quick and it had formed disordered columns as shown in the cross section [Fig. 2(b)]. On the other hand, when the applied potential is less negative [−0.7 V, Figs. 2(c) and 2(d)], the obtained film is thinner, more compact, and presents a clearer order. The morphology of the film at $-0.7$ V presents columnar and two-dimensional growth. For the least negative potential in which it has been possible to obtain a deposit [−0.6 V, Figs. 2(e) and 2(f)], the surface of the film is the smoothest. As can be seen in Figs. 2(b), 2(d), and 2(f), the thickness of the deposit was around 30 $\mu$m for $-1$ V, around 4 $\mu$m for $-0.7$ V, and around 0.4 $\mu$m for $-0.6$ V.

Figure 3 shows the XRD patterns of the ZnO films deposited in the above-mentioned conditions. The intensity has been displayed in log scale to enhance small diffraction peaks. It can be seen that the film is purely made of ZnO, because the peaks to be seen are only the ones from the substrate (Si with a 150 nm Au layer) and two of ZnO, (0002) and (0004), indicating that only one crystalline direction of ZnO is present in the film. The films are textured along the [001] direction, due to the coalescence of individual hexagonal grains. The full width at half maximum (FWHM) of these curves is presented in Table I. The FWHM is smaller (0.115 vs 0.17) for films electrodeposited at the more negative potential. This is related to the fact that more negative potentials give bigger ZnO grain sizes.

TABLE I. Parameters from XRD analysis.

| Solution | *E* (V) | FWHM |
|---|---|---|
| Nitrate | −1.0 | 0.115 |
| Nitrate | −0.7 | 0.158 |
| Nitrate | −0.6 | 0.170 |
| Peroxide | −0.9 | 0.158 |
| Peroxide | −0.5 | 0.170 |
| Peroxide | −0.3 | 0.172 |

### 2. Peroxide solution

The morphology of the films obtained with this solution can be seen in scanning electron microscopy images (Fig. 4) for different potentials. The film grown at the most negative potential [−0.9 V, Fig. 4(a)] presents hexagonal columns. These columns are aligned perpendicularly to the substrate's surface, as shown in the cross-sectional micrograph of this film in Fig. 4(b), where a clear columnar growth can be seen. This is due again to the coalescence of individual hexagonal grains. In other words, it is a nucleation-growth mechanism. Figures 4(c) and 4(d) display the SEM images of the ZnO film electrodeposited at $-0.5$ V. The cross section [Fig. 4(d)] shows a columnar growth, but the grains are not hexagonal as in the case of the nitrite solution [see the top view Fig. 4(c)]. For the least negative potential [−0.3 V, Figs. 4(e) and 4(f)], the film obtained has the smoothest surface found for this solution, and columns are not observed. For lower potentials than $-0.3$ V, no deposit was obtained.

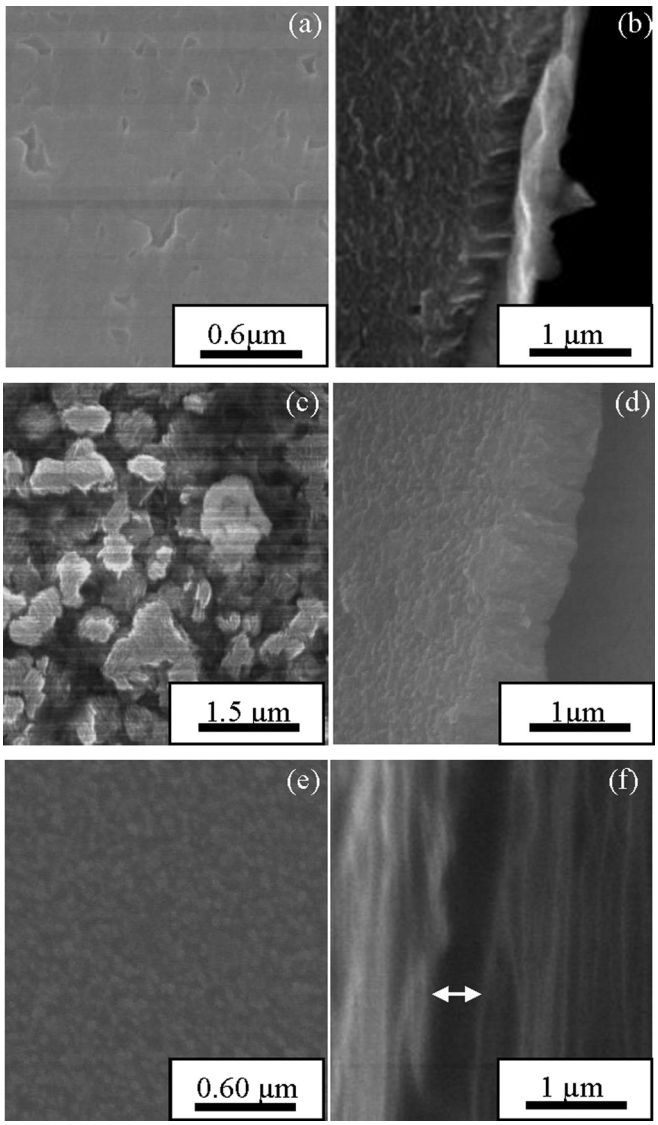


FIG. 4. SEM images of the films electrodeposited in the peroxide solution for 1 h; (a) $-0.9$ V top view; (b) $-0.9$ V 45° tilted view; (c) $-0.5$ V top view; (d) $-0.5$ V 45° tilted view; (e) $-0.3$ V top view; (f) $-0.3$V cross sectional, the arrow marks the film thickness.

In order to study the crystalline quality of the films grown in the peroxide solution, XRD was taken (see Fig. 5). As in the previous case, only the diffraction peaks of ZnO in the [0001] direction can be seen for the films electrodeposited at – 0.9, – 0.5, and – 0.3 V. That means that the films are textured along this direction. However, the XRD pattern of the film electrodeposited at – 0.3 V shows only one peak of ZnO, (0002). The (0004) peak is not observed in the XRD pattern. Table I lists the values of the FWHM of ZnO films electrodeposited in peroxide solution. As in the previous case, the film electrodeposited at the least negative potential (−0.3 V) presents smaller grain size (bigger FWHM).

It is interesting to note here that the films obtained at more negative potentials are thinner for the same total area than films grown at less negative potentials [see Figs. 4(b), 4(d), and 4(f)].

A possible explanation for that is, in the case of electrochemical deposition performed at very negative potentials and/or large hydrogen peroxide concentration, that Eq. (6d) will be the dominant one. In these cases, the $OH^-$ formed at the surface of the electrode is desorbed from the electrode and will react in the solution with $Zn^{2+}$ forming $Zn(OH)_2$ powder out of the electrode, which will react at temperature >50 °C to form ZnO. The experimental observation of this reaction is obtained by looking at the electrodeposition cell during deposition. A white precipitate appears in the solution going from a position close to the working electrode to the bottom of the electrochemical cell. This causes a very slow but rather ordered growth. The white precipitate does not appear at less negative potentials. As can be seen in Figs. 4(b) and 4(f), the thickness of the deposit for the same area (0.196 $cm^2$) was around 0.3 $\mu$m for – 0.9 V and around 0.6 $\mu$m for – 0.3 V. This highlights that the Faradaic efficiency of the system is higher for – 0.3 V, since for more negative potentials not all the $OH^-$ produced at the electrode surface generates ZnO deposit.

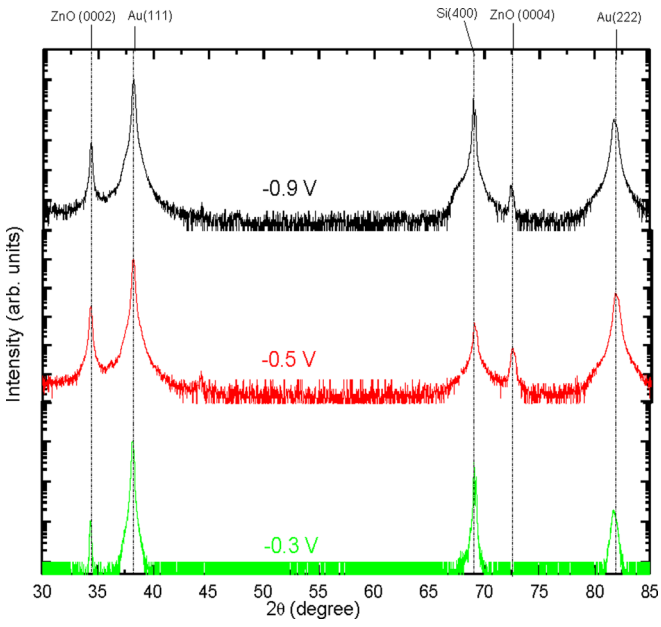


FIG. 5. (Color online) XRD patterns of the ZnO films grown in the peroxide solution at different voltages: – 0.9, – 0.5, and – 0.3 V vs Ag/AgCl.

### C. Crystalline defects: Photoluminescence

In the case of ZnO, the bandgap emission appears in the near ultraviolet around 370–385 nm (3.3 eV). All the studied films show PL in the visible region between 400 and 900 nm, as shown in Fig. 6. This broad band can be related to the presence of different defects (and/or impurities) with different concentrations in each sample. A deconvolution into four Gaussian peaks has been used in Ref. 31 to describe this visible emission in ZnO: a green component centered at 515 nm (2.41 eV); a yellow at 560 nm (2.21 eV); an orange-red centered at 670 nm (1.85 eV), and a tail in the infrared centered at 785 nm (1.58 eV). The resulting areas for each component are presented in Fig. 7 for the different samples of our study.

In the literature, there is a great controversy in the assignation of defects to the different emission lines (see Ref. 41 for instance). This disagreement is mainly due to two reasons: (1) the wide and rather unstructured character of the emission between 400 and 900 nm; and (2) many defects can be present in the sample at the same time.[41,42]

There are many theoretical studies about the transition levels of the defects in ZnO.[43–46] Among them, we have chosen the most recent and complete study presented by Janotti and Van de Walle[42] in order to explain our results. According to this study, the typology of defects that most probably could be found in ZnO films grown under oxygen-rich conditions are intrinsic defects like zinc vacancies ($V_{Zn}$), interstitial oxygen ($O_i$), and oxygen antisites ($O_{Zn}$).[42] Moreover, taking into account that the films grown by electrodeposition are generated according to reaction (1), extrinsic defects like trapped $OH^-$ should also be taken into account. This type of defect is known as H-I.[47]

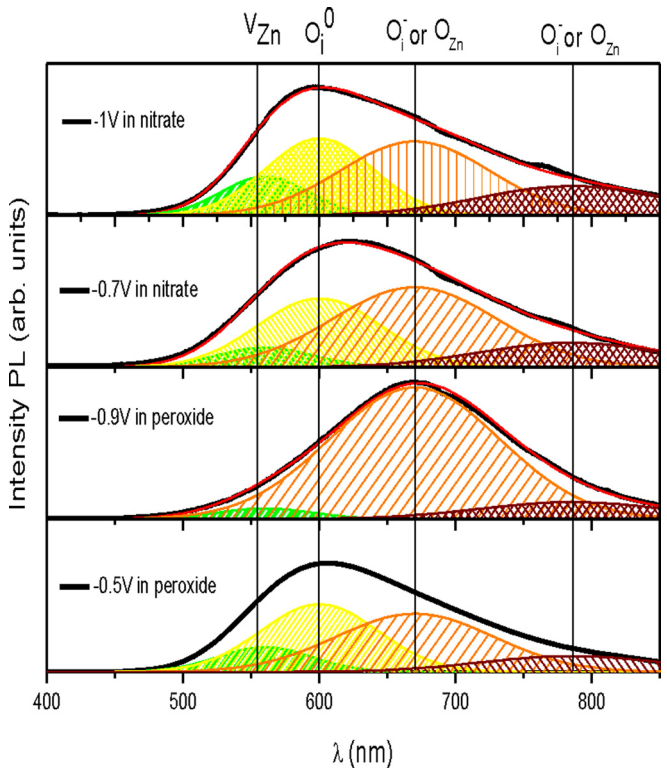


FIG. 6. (Color online) Gaussian deconvolution of the visible emission of electrodeposited ZnO films grown under different conditions.

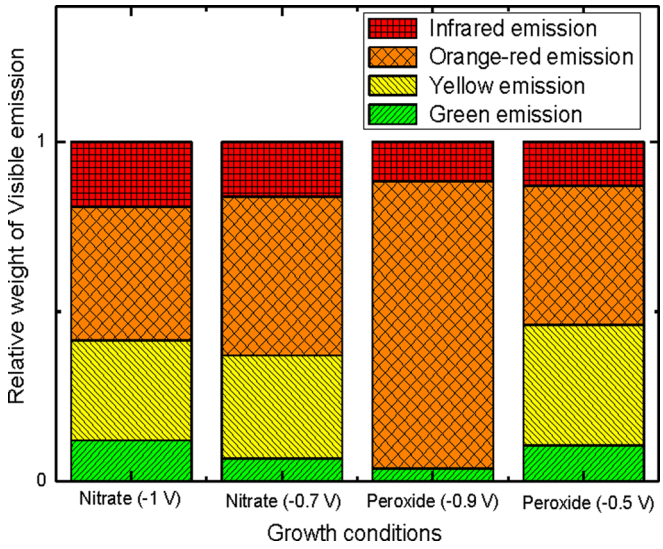


FIG. 7. (Color online) Relative weight of the different Gaussian components deconvoluted from the visible emission of the electrodeposited ZnO films grown under different conditions. Total area normalized to 1.

Figure 8 represents the proposed model for the photoluminescence emissions of the electrodeposited ZnO films. It is important to note that the energy of the donor extrinsic defect $OH^-$ (H-I) also has been added to the graph from Refs. 46 and 47 for completeness. The proposed transitions have been marked as arrows and identified with their emission color.

The *green and yellow emissions* are tentatively assigned to a transition from the donor $OH^-$ to the acceptor zinc vacancies ($V_{Zn}^-$) and interstitial oxygen ($O_i^0$), respectively. Since recent results suggest that both yellow and green emissions are present in samples grown in solution, they are both related to a transition from the same donor to different acceptors placed at different depths in the energy level scheme.[48] The existence of this kind of shallow donor has been long known in samples grown in solution,[49] but its nature is more difficult to clarify. They have been related to $V_O$,[9,50] but the theoretical calculations by Janotti and Van de Walle[42] indicate that $V_O$ defects form rather deep levels, as

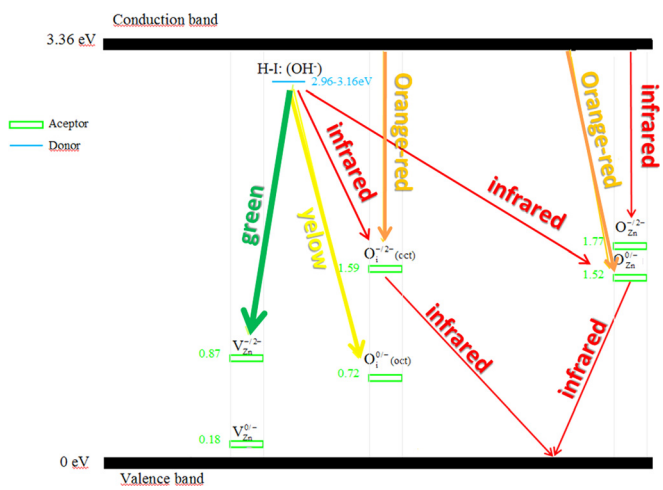


FIG. 8. (Color online) Proposed transitions related to defect emission in the visible range (Refs. 32 and 36).

can be seen in Fig. 8. Given that no other intrinsic defect appears at a shallow position in the energy scheme, this characteristic must be attributed to an extrinsic defect. As was mentioned before, the only extrinsic defects expected in our samples are hydrogen-related defects, like the H-I. The energy proposed in the literature for this defect is 2.91 eV,[46,47] which means that it can be considered as a shallow donor. Moreover, the best evidence that can be given is the absence of the yellow band and most of the green band, in the spectrum emitted from the sample that has been electrodeposited at the slowest growth rate (−0.9 V in the peroxide solution), as shown in Fig. 7. Due to the $OH^-$ desorption under these conditions [see Eq. 6(d)], this sample is expected to have the smallest amount of trapped $OH^-$, and therefore of H-I defects. It should be noted that while the yellow emission disappears completely, the green band is not fully attenuated in the spectrum. Recent works have reported, via positron annihilation spectroscopy,[51,52] the presence of zinc vacancies ($V_{Zn}^-$) surrounded by a variable number of OH bonds in these kind of samples. This justifies the choosing of $V_{Zn}^-$ as the acceptor in the green emission transition, because $OH^-$ stabilizes this kind of vacancy. Our association of the green and yellow emissions to transitions from the H-I defect (or trapped $OH^-$) to $O_i^0$ and $V_{Zn-}$, respectively, can be further clarified by annealing the samples at 110 °C. At this temperature the H-I defects start to disappear slowly[48] with the subsequent reduction in the green and yellow emission as shown in Figs. 9 and 10. Raising the annealing temperature to 150 °C, the H-I defects are further reduced and at temperatures higher than 250 °C, the green emission is no longer observed.

The *orange-red emission* corresponding to an energy of 1.85 eV (670 nm) has been traditionally assigned to an excess of oxygen.[53] In our case, we have always attributed the excess of oxygen to the growth technique, but the literature does not specify which of the multiple oxygen defects present in ZnO is implied, only that the electron is de-excited from the conduction band.[51] Taking into account the

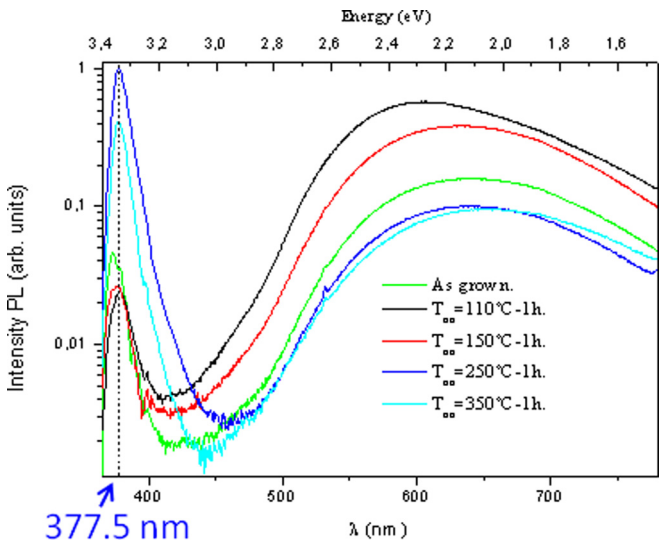


FIG. 9. (Color online) Photoluminescence measured (in log scale) at room temperature of the sample grown at − 0.5 V in the peroxide solution, as grown and annealed at different temperatures.

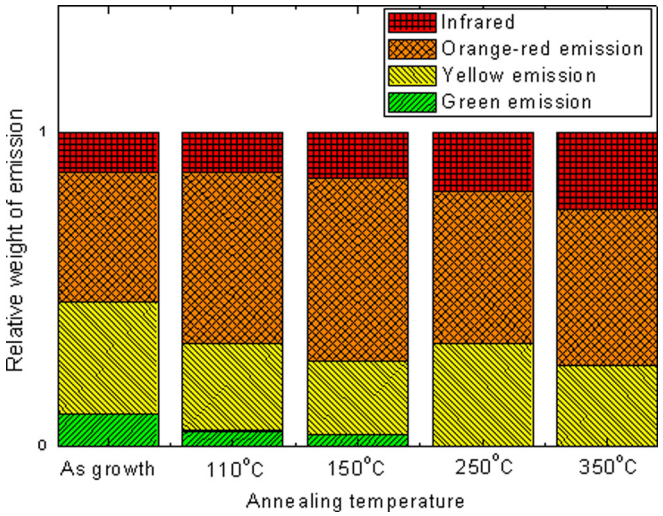


FIG. 10. (Color online) Relative weight for the Gaussian components deconvoluted from the emission of the electrodeposited ZnO film (grown at – 0.5 V in the peroxide solution). Total area normalized to 1.

theoretical transition values shown in Fig. 8,[42] a transition of 1.85 eV is found for electrons coming from the conduction band toward $O_i^-$ and $O_{Zn}^0$ defects (the transition is represented with orange arrows in Fig. 8). In our samples, both defects are expected to be present and, given that their energy levels are quite similar, we can conclude that both of them can be responsible for this emission. The films electrodeposited at slower growth rates (potential of – 0.9 V for the peroxide solution and – 0.7 V for the nitrate solution) present a more important orange-red component (see Fig. 7). This could be explained if one or both $O_{Zn}$ and $O_i$ are favored at slower deposition velocities.

The *infrared emission* corresponding to energy of 785 nm (1.58 eV) might be due to a transition from the defects $O_i^{-/2-}$ and $O_{Zn}^{0/-}$ to the valence band or a transition from the conduction band to $O_{Zn}^{-/2-}$, or even the transition from the H-I defect to $O_i^{-/2-}$ and $O_{Zn}^{0/-}$. All of them have an energy around the infrared values obtained, which are represented in Fig. 8 as red arrows. As can be seen there, these infrared transitions complete the deexcitation path of the electrons that made a first deexcitation transition by emitting orange-red light. This infrared emission increases at annealing temperatures above 350 °C (see Fig. 10). This can be explained following

$$O_i + V_{Zn} \rightarrow O_{Zn}, \quad (7)$$

Ref. 54. This new $O_{Zn}$ defect created as a consequence of the annealing is responsible for the emission increase found in our experiments.

*The bandgap emission* was detected in the spectra of all samples with exactly the same energy (3.363 eV) (see Fig. 9). It is worth mentioning that this ultraviolet emission is quite rare in the case of electrodeposited samples. The explanation of its appearance at room temperature can be the presence of bound excitons. Its contribution increases when the samples are annealed. Moreover, when the annealing temperature is 250 °C, the emission is enhanced 40 times. For higher temperatures the bandgap emission starts to decrease probably due to the creation of new defects, possibly $V_O$.[51]

In summary, we have associated the *green and yellow emissions* to a transition from the donor $OH^-$ to the acceptor zinc vacancies ($V_{Zn}^-$) and interstitial oxygen ($O_i^0$), respectively. The *orange-red emission* is probably due to transitions from the conducting band to $O_i^-$ and $O_{Zn}^0$ defects and the *infrared emission* to transition from these $O_i^{-/2-}$ and $O_{Zn}^{0/-}$ defects to the valence band.

## IV. CONCLUSIONS

In this paper we have obtained high quality films of ZnO growth via electrodeposition at constant potentials from two different solutions (nitrate and peroxide). The reactions that give rise to the electrodeposition process have been described. The morphological analysis of the grown films showed good control over their morphology depending on the electrodeposition conditions. X-ray diffraction spectra showed that the films were oriented with the *c* axis perpendicular to the substrate (along the [001] direction). Moreover, the defects present in the different films have been studied with photoluminescence experiments. The possible origins of the different emission transitions that are present in these ZnO electrodeposited films have been determined, with the aid of their relative intensities after the deconvolution of the complete spectra and their behavior after annealing treatments. The defects present in our films are H-I defects, zinc vacancies, and interstitial oxygen and antisite oxygen. The first one acts as a shallow donor that gives rise to transitions that revert in green light emission when combined with zinc vacancies, and yellow light emission when interstitial oxygen act as acceptors. Then, the orange-red emission consists of transitions between the conduction band and interstitial or antisite oxygen. Finally, the infrared emission consists in transition from interstitial oxygen or antisite oxygen defects to the valence band. It is also worth mentioning that these films also present emission in the ultraviolet range, which is quite difficult to obtain in the case of electrodeposited samples. This transition can be associated with the presence of bound excitons in the as-grown films, where its contribution is greatly enhanced when annealed at 250 °C.

## ACKNOWLEDGMENTS

The authors would like to acknowledge partial financial support from MICINN Project No. MAT2008-06330 and ERC StG NanoTEC 240497. C.V.M. wants to acknowledge CSIC for JAE PhD grant, and O.C.C. wants to acknowledge CSIC for JAE post-doctoral position.

[1] C. H. Ahn, Y. Y. Kim, D. C. Kim, S. K. Mohanta, and H. K. Cho, J. Appl. Phys. **105**, 013502 (2009).
[2] H. T. Wang, B. S. Kang, F. Ren, L. C. Tien, P. W. Sadik, D. P. Norton, S. J. Pearton, and J. Lin, Appl. Phys. Lett. **86**, 243503 (2005).
[3] S. M. Al-Hilli, R. T. Al-Mofarji, P. Klason, M. Willander, N. Gutman, and A. Sa'ar, J. Appl. Phys. **103**, 014302 (2008).
[4] U. Ozgur, Y. I. Alivov, C. Liu, A. Teke, M. A. Reshchikov, S. Dogan, V. Avrutin, S.-J. Cho, and H. Morkoc, J. Appl. Phys. **98**, 041301 (2005).
[5] C. Klingshirn; Phys. Stat. Sol. (b) 244, 3027 (2007).
[6] T. Tsubota, M. Ohtaki, K. Eguchi, and H. Arai, J. Mater. Chem. **7**, 85 (1997).

[7]M. A. Garcia, A. Quesada, J. L. Costa-Krämer, J. F. Fernández, S. J. Khatib, A. Wennberg, A. C. Caballero, M. S. Martín-González, M. Villegas, F. Briones, J. M. González-Calbet, and A. Hernando, Phys. Rev. Lett. **94**, 217206 (2005).
[8]A. Serrano, E. F. Pinel, A. Quesada, I. Lorite, M. Plaza, L. Pérez, F. Jiménez-Villacorta, J. de la Venta, M. S. Martín-González, J. L. Costa-Krämer, J. F. Fernandez, J. G. Llopis, and M. A. Garcia, Phys. Rev. B **79**, 144405 (2009).
[9]J. F. Fernández, A. C. Caballero, M. Villegas, S. J. Khatib, M. A. Bañares, J. L. G. Fierro, J. L. Costa-Kramer, E. Lopez-Ponce, M. S. Martín-González, F. Briones, A. Quesada, M. García, and A. Hernando, J. Eur. Ceram. Soc. **26**, 3017 (2006).
[10]M. S. Martin-Gonzalez, J. F. Fernandez, F. Rubio-Marcos, I. Lorite, J. L. Costa-Kramer, A. Quesada, M. A. Banares, and J. L. G. Fierro, J. Appl. Phys. **103**, 083905 (2008).
[11]M. S. Martin-Gonzalez, M. A. Garcia, I. Lorite, J. L. Costa-Kramer, F. Rubio-Marcos, N. Carmona, and J. F. Fernandez, J. Electrochem. Soc. **157**, E31 (2010).
[12]M. S. Martín-Gonzalez, C. S. Steplecaru, F. Briones, E. López-Ponce, J. F. Fernández, M. A. García, A. Quesada, C. Ballesteros, and J. L. Costa-Krämer, Thin Solid Films **518**, 4607 (2010).
[13]W. Lee, M.-C. Jeong, and J.-M. Myoung, Acta Mater. **52**, 3949 (2004).
[14]S. Yanagida, G. K. R. Senadeera, K. Nakamura, T. Kitamura, and Y. Wada, J. Photochem. Photobiol., A: **166**, 75 (2004).
[15]Y. Gao and M. Nagai, Langmuir **22**, 3936 (2006).
[16]M. Willander O. Nur, Q. X. Zhao, L. L. Yang, M. Lorenz, B. Q. Cao, J. Zúñiga Pérez, C. Czekalla, G. Zimmermann, M. Grundmann, A. Bakin, A. Beherends, M. Al-Suleiman, A. El-Shaer, A. Che. Mofor, B. Postels, A. Waag, N. Boukos, A. Travlos, H. S. Kwack, J. Guinard, and D. Le Si Dang, Nanotechnology **20**, 332001 (2009).
[17]S. Kishwar, K. ul Hasan, N. H. Alvi, P. Klason, O. Nur, and M. Willander, Superlattices Microstruct. **49**, 32 (2011).
[18]Z. P. Wei, Y. M. Lu, D. Z. Shen, Z. Z. Zhang, B. Yao, B. H. Li, J. Y. Zhang, D. X. Zhao, X. W. Fan, and Z. K. Tang, Appl. Phys. Lett. **90**, 042113 (2007).
[19]W. Liu, S. L. Gu, J. D. Ye, S. M. Zhu, S. M. Liu, X. Zhou, R. Zhang, Y. Shi, Y. D. Zheng, Y. Hang, and C. L. Zhang, Appl. Phys. Lett. **88**, 092101 (2006).
[20]Y. R. Ryu, T. S. Lee, J. A. Lubguban, H. W. White, Y. S. Park, and C. J. Youn, Appl. Phys. Lett. **87**, 153504 (2005).
[21]A. Tsukazaki, A. Ohtomo, T. Onuma, M. Ohtani, T. Makino, M. Sumiya, K. Ohtani, S. F. Chichibu, S. Fuke, Y. Segawa, H. Ohno, H. Koinuma, and M. Kawasaki, Nature Mater. **4**, 42 (2005).
[22]Y. Ryu, T.-S. Lee, J. A. Lubguban, H. W. White, B.-J. Kim, Y.-S. Park, and C.-J. Youn, Appl. Phys. Lett. **88**, 241108 (2006).
[23]T. Aoki, Y. Hatanaka, and D. C. Look, Appl. Phys. Lett. **76**, 3257 (2000).
[24]Z. Z. Ye, J. G. Lu, Y. Z. Zhang, Y. J. Zeng, L. L. Chen, F. Zhuge, G. D. Yuan, H. P. He, L. P. Zhu, J. Y. Huang, and B. H. Zhao, Appl. Phys. Lett. **91**, 113503 (2007).
[25]T. Pauportéand D. Lincot, Electrochim. Acta **45**, 3345 (2000).
[26]S. Peulon and D. Lincot, J. Electrochem. Soc. **145**, 864 (1998).
[27]T. Pauporté and D. Lincot, J. Electroanal. Chem. **517**, 54 (2001).
[28]S. Peulon and D. Lincot, Adv. Mater. **8**, 166 (1996).
[29]M. Izaki and T. Omi, Appl. Phys. Lett. **68**, 2439 (1996).
[30]T. Pauporté and D. Lincot, J. Electrochem. Soc. **148**, C310 (2001).
[31]M. S. Martin-Gonzalez, J. Garcia-Jaca, E. Moran, and M. A. Alario-Franco, J. Mater. Chem. **9**, 137 (1999).
[32]M. Martin-Gonzalez, E. Moran, O. Rodriguez de la Fuente, and M. A. Alario-Franco, J. Mater. Chem. **11**, 616 (2001).
[33]M. J. N. Pourbaix, *Atlas of Electrochemical Equilibria in Aqueous Solutions* (Pergamon, New York, 1966).
[34]T. Mahalingam, V. S. John, M. Raja, Y. K. Su, and P. J. Sebastian, Sol.Energy Mater. Sol. Cells **88**, 227 (2005).
[35]M. Lai, Chem. Mater. **18**, 2233 (2006).
[36]S. Karuppuchamy, K. Nonomura, T. Yoshida, T. Sugiura, and H. Minoura, Solid State Ionics **151**, 19 (2002).
[37]X. Han, R. Liu, W. Chen, and Z. Xu, Thin Solid Films **516**, 4025 (2008).
[38]T. Ren, H. R. Baker, and K. M. Poduska, Thin Solid Films **515**, 7976 (2007).
[39]T. Yoshida, D. Komatsu, N. Shimokawa, and H. Minoura, Thin Solid Films **451–452**, 166 (2004).
[40]J. Yu and M. Kupferle Water, Air, Soil Pollut. **9**, 245 (2009).
[41]A. B. Djurišić and Y. H. Leung, Small (Wiley-VCH, Weinheim, 2006), Vol. **2**, p. 944.
[42]A. Janotti and C. G. Van de Walle, Phys. Rev. B **76**, 165202 (2007).
[43]P. S. Xu, Y. M. Sun, C. S. Shi, F. Q. Xu, and H. B. Pan, Nucl. Instrum. Methods Phys. Res. B **199**, 286 (2003).
[44]S. A. M. Lima, F. A. Sigoli, M. JafelicciJr., and M. R. Davolos, Int. J. Inorg. Mater., **3**, 749 (2001).
[45]B. Lin, Z. Fu, Y. Jia, and G. Liao, J. Electrochem. Soc. **148**, G110 (2001).
[46]E. V. Lavrov, J. Weber, F. Börrnert, C. G. Van de Walle, and R. Helbig, Phys. Rev. B **66**, 165205 (2002).
[47]E. V. Lavrov, F. Börnert, and J. Weber, Phys. Rev. B **72**, 085212 (2005).
[48]R. B. Lauer, J. Phys. Chem. Solids **34**, 249 (1973).
[49]J. C. Simpson, J. F. Cordora, J. Appl. Phys. **63**, 1781 (1998).
[50]K. Kuriyama, M. Ooi, K. Matsumoto, and K. Kushida, Appl. Phys. Lett. **89**, 242113 (2006).
[51]J. Cizek, N. Zaludova, M. Vlach, S. Danis, J. Kuriplach, I. Prochazka, G. Brauer, W. Anwand, D. Grambole, W. Skorupa, R. Gemma, R. Kirchheim, and A. Pundt, J. Appl. Phys. **103**, 053508 (2008).
[52]G. Brauer, J. Kuriplach, J. Cizek, W. Anwand, O. Melikhova, I. Prochazka, and W. Skorupa, Vacuum **81**, 1314 (2007).
[53]A. B. Djurisic, Y. H. Leung, K. H. Tam, L. Ding, W. K. Ge, H. Y. Chen, and S. Gwo, Appl. Phys. Lett. **88**, 103107 (2006).
[54]Y. Yang, H. Yan, Z. Fu, B. Yang, L. Xia, Y. Xu, J. Zuo, and F. Li Solid State Commun., **138**, 521 (2006).